Monthly Notices of the ROYAL ASTRONOMICAL SOCIETY

MNRAS **507,** 5690–5702 (2021) https://doi.org/10.1093/mnras/stab2425
Advance Access publication 2021 August 28

X-ray spectra, light curves and SEDs of blazars frequently observed by Swift

Paolo Giommi [1,2,3,4]★ M. Perri,[5,6] M. Capalbi,[7] V. D'Elia,[5,8] U. Barres de Almeida,[9] C. H. Brandt,[4,9,10] A. M. T. Pollock,[11] F. Arneodo,[12] A. Di Giovanni,[12] Y. L. Chang,[13] O. Civitarese,[14,15] M. De Angelis,[8] C. Leto,[8] F. Verrecchia,[5,6] N. Ricard,[16] S. Di Pippo,[16] R. Middei [5] A. V. Penacchioni,[14] R. Ruffini,[4,17] N. Sahakyan,[4,17,18] D. Israyelyan[18] and S. Turriziani [19]

[1]*Institute for Advanced Study, Technische Universität München, Lichtenbergstrasse 2a, Garching bei München D-85748, Germany*
[2]*Associated to Italian Space Agency, ASI, via del Politecnico snc, Roma 00133, Italy*
[3]*Center for Astro, Particle and Planetary Physics (CAP3), New York University Abu Dhabi, Abu Dhabi PO Box 129188, United Arab Emirates*
[4]*ICRANet, P.zza della Repubblica 10, Pescara 65122, Italy*
[5]*Space Science Data Center, SSDC, ASI, via del Politecnico snc, Roma 00133, Italy*
[6]*INAF - Osservatorio Astronomico di Roma, via di Frascati 33, Monteporzio Catone I-00078, Italy*
[7]*INAF - Istituto di Astrofisica Spaziale e Fisica Cosmica di Palermo, via Ugo La Malfa 153, Palermo I-90146, Italy*
[8]*Italian Space Agency, ASI, via del Politecnico snc, Roma 00133, Italy*
[9]*Centro Brasileiro de Pesquisas Físicas, Rua Dr. Xavier Sigaud 150, Rio de Janeiro 22290-180, Brazil*
[10]*Physics and Earth Sciences, Jacobs University, Campus Ring 1, Bremen 28759, Germany*
[11]*Department of Physics and Astronomy, University of Sheffield, Hounsfield Road, Sheffield S3 7RH, England*
[12]*Division of Science and Center for Astro, Particle, and Planetary Physics, New York University Abu Dhabi, Saadiyat Island, Abu Dhabi 129188, UAE*
[13]*Tsung-Dao Lee Institute, Shanghai Jiao Tong University, 800 Dongchuan RD. Minhang District, Shanghai, China*
[14]*Institute of Physics, IFLP-CONICET, diag 113 e/63-64.(1900) La Plata, Argentina*
[15]*Department of Physics, University of La Plata, 49 and 115.C.C.67 (1900) La Plata, Argentina*
[16]*United Nations Office for Outer Space Affairs, UNOOSA, Vienna A-1220, Austria*
[17]*ICRA, Dipartimento di Fisica, Sapienza Universita' di Roma, P.le Aldo Moro 5, Rome 00185, Italy*
[18]*ICRANet-Armenia, Marshall Baghramian Avenue 24a, Yerevan 0019, Armenia*
[19]*Physics Department, Gubkin Russian State University (National Research University), 65 Leninsky Prospekt, Moscow 119991, Russian Federation*

Accepted 2021 August 16. Received 2021 August 9; in original form 2021 May 17

ABSTRACT

Blazars research is one of the hot topics of contemporary extragalactic astrophysics. That is because these sources are the most abundant type of extragalactic γ-ray sources and are suspected to play a central role in multimessenger astrophysics. We have used Swift_xrtproc, a tool to carry out an accurate spectral and photometric analysis of the Swift-XRT data of all blazars observed by Swift at least 50 times between December 2004 and the end of 2020. We present a database of X-ray spectra, best-fit parameter values, count rates and flux estimations in several energy bands of over 31 000 X-ray observations and single snapshots of 65 blazars. The results of the X-ray analysis have been combined with other multifrequency archival data to assemble the broad-band Spectral Energy Distributions (SEDs) and the long-term light curves of all sources in the sample. Our study shows that large X-ray luminosity variability on different time-scales is present in all objects. Spectral changes are also frequently observed with a 'harder-when-brighter' or 'softer-when-brighter' behaviour depending on the SED type of the blazars. The peak energy of the synchrotron component ($\nu_{\rm peak}$) in the SED of HBL blazars, estimated from the log-parabolic shape of their X-ray spectra, also exhibits very large changes in the same source, spanning a range of over two orders of magnitude in Mrk421 and Mrk501, the objects with the best data sets in our sample.

Key words: methods: data analysis – Astronomical data bases: catalogues – galaxies: active – galaxies: BL Lacertae objects – quasars: general – X-rays: galaxies.

1 INTRODUCTION

Blazars are the most powerful non-explosive sources in the Universe. What makes these sources special compared to other types of Active Galactic Nuclei (AGN, Padovani et al. 2017) is that their electromagnetic emission is dominated by non-thermal radiation that is generated within a jet that moves away from the central supermassive black hole at relativistic speeds and points in the direction of the Earth (see e.g. Blandford & Rees 1978; Urry & Padovani 1995; Padovani et al. 2017).

Blazars are sub-classified as Flat-Spectrum Radio Quasars (FSRQs) and BL Lacertae objects (or BL Lacs), based on their optical spectra: FSRQs show broad emission lines like radio-quiet Quasi-

★ E-mail: giommipaolo@gmail.com

Stellar Objects, while BL Lacs display at most very weak emission lines, and in several cases are completely featureless (e.g. Falomo, Pian & Treves 2014).

The radio to γ-ray Spectral Energy Distribution of blazars [SED, a plot of the $\nu f(\nu)$ flux as a function of frequency ν] always displays a 'double humped' shape (see e.g. Abdo et al. 2010; Giommi et al. 2012). The low-energy hump, peaking between the far-IR and the X-ray band, is generally attributed to synchrotron radiation produced by relativistic particles moving in a magnetic field inside the jet. The second component, which spans from the X-rays to the γ-ray band, is usually explained as inverse Compton scattering of the electrons against synchrotron generated photons, or other photon field. Depending on whether the peak of the synchrotron part of the SED ($\nu_{\rm peak}$) is located at low, intermediate, or high frequencies (or energy) blazars have been classified as objects of the LBL, IBL, or HBL type,[1] originally for BL Lac objects only (Padovani & Giommi 1995). This classification was subsequently extended to FSRQs by Abdo et al. (2010) who used the LSP, ISP, and HSP coding. In this paper, we adopt the original LBL, IBL, and HBL codification for all blazars types.

Blazars are central to today's extragalactic high-energy astrophysics as they are by far the most common type of γ-ray sources at high Galactic latitudes (Abdollahi et al. 2020; Ballet et al. 2020), and are expected to be abundantly detected in the very high-energy ($E \gtrsim 50$ GeV) γ-ray sky that will soon be surveyed by a new generation of VHE observatories such as Cherenkov Telescope Array (CTA Consortium et al. 2019) and LHAASO (La Mura et al. 2020).[2] Blazars have also been proposed to play a key role in the emerging field of multimessenger astrophysics (e.g. Mannheim 1995; Resconi et al. 2017), and their relevance in this area is growing after the association of the object TXS0506 + 056, and possibly several other blazars, with some IceCube astrophysical high-energy neutrinos (e.g. IceCube Collaboration et al. 2018; Padovani et al. 2018; Giommi et al. 2020b).

As part of the Open Universe initiative (Giommi et al. 2020a) we have recently started a series of activities aiming at the generation of transparent scientific products from multifrequency data obtained by the Neil Gehrels Swift observatory (Gehrels et al. 2004, hereafter Swift) and other astronomy satellites. One such program, Open Universe for blazars,[3] is dedicated to the class of blazars.

Open Universe is an initiative of the United Nations Office for Outer Space Affairs (UNOOSA) with the objective of making astronomy and space science data more openly available, easily discoverable, free of bureaucratic, administrative or technical barriers, and therefore, usable by the widest possible community, from professional researchers to all people interested in space science. In addition to generating impact on education and capacity building for the XXI Century, one of the main goals of Open Universe is to increase the productivity of space research. By doing so, it aims to contribute to the democratisation of space science and to the achievement of some of the United Nations Sustainable Development Goals. The Initiative, initially proposed by Italy to the Committee On the Peaceful Uses of Outer Space in 2016, is now under implementation within UNOOSA, with the contribution of a number of scientists and institutions from various countries.

In an earlier paper (Giommi et al. 2019, hereafter Paper I), we presented a new generation of astronomical products for all the catalogued blazars observed by Swift-XRT during its first 14 years of activity. In this paper, we present a detailed X-ray spectral, imaging and timing analysis of all the observations and single snapshots[4] of a sample of 65 blazars that have been observed by Swift more than 50 times over a period of 16 years, from launch to the end of 2020. The resulting science-ready data products are used to compile the SED and X-ray light curve of each source in the sample. A preliminary version of this project was presented by Giommi (2015) on the occasion of the tenth anniversary of the launch of the Swift mission. All the results are available through the Open Universe platform, the ASI Space Science Data Center (SSDC), the Virtual Observatory (VO), and through other data release methods. In particular, all the SED data points and light curves are accessible through the VOU-blazars tool (Chang, Brandt & Giommi 2020).

This work is meant to be a contribution to the goal of creating a high-transparency database, dedicated to blazars, based on the most advanced principles of open data access and behavioural insight approaches.[5]

The paper is structured as follows. In Section 2, we introduce the sample, in Section 3, we describe in detail the data analysis, in Section 4, we present the results of the analysis of the XRT data, together with the broad-band SEDs and X-ray light curves. In Section 5, we discuss the results.

2 BLAZARS FREQUENTLY OBSERVED BY SWIFT-XRT

Although specifically designed for Gamma Ray Burst science, Swift has proven to be an extremely effective multipurpose multifrequency observatory. A large number of bright and highly variable X-ray sources have been observed many times between launch in November 2004, and the end of 2020. The list of blazars that have been observed at least 50 times in this period with the X-ray telescope (XRT, Burrows et al. 2005) is given in Table 1, where column 1 is the source common or historical name, column 2 is the name of the object in the BZCAT (Massaro et al. 2015) or the 3HSP (Chang et al. 2019) catalogues, or following the IAU denomination in case the object is not listed in these two catalogues, column 3 gives the SED classification of the blazar (LBL, IBL, or HBL), column 4 gives the number of XRT observations with exposure larger than 200 s in Photon Counting (PC) or Windowed Timing (WT) mode (see Burrows et al. 2005, for details of the readout modes), column 5 gives the ratio between the minimum and maximum flux observed at 1 keV. The list includes 65 objects, 24 of which are HBLs, 12 are IBLs and 29 are LBLs. The sky distribution of the sub-sample of sources observed more than 100 times shown in Fig. 1 shows that the blazars most pointed by Swift are mostly located in the Northern sky.

Although the data presented in this paper is probably the largest available set of homogeneous X-ray measurements of blazars, it is far from being a collection of observations carried out at random times on a sample of randomly selected sources that would be needed for an unbiased view of blazars. Any statistical consideration based on the

[1]LBL: $\nu_{\rm peak} < 10^{14}$ Hz; IBL: 10^{14} Hz $< \nu_{\rm peak} < 10^{15}$ Hz; HBL: $\nu_{\rm peak} > 10^{15}$ Hz.
[2]http://english.ihep.cas.cn/lhaaso
[3]https://sites.google.com/view/ou4blazars
[4]A Swift observation snapshot is the time interval spent continuously observing a target. A complete observation is composed of one or more snapshots sharing the same observation ID
[5]https://www.oecd.org/gov/regulatory-policy/behavioural-insights.htm

Table 1. The sample of blazars observed by Swift-XRT in PC or WT mode more than 50 times from launch in November 2004 to November 2020. See Section 2 for a description of the columns.

Common or discovery name (1)	5BZB or 3HSP IAU denomination (2)	SED type (3)	Obs. with good spectra (4)	f_{max}/f_{min} @1 keV (5)
1ES0033 + 595	3HSPJ003552.6 + 595004	HBL	141	8.3
PKS0208 − 512	5BZUJ0210-5101	LBL	161	31.7
3C 66A	5BZBJ0222 + 4302	IBL	109	16.2
1ES0229 + 200	3HSPJ023248.6 + 201717	HBL	80	3.8
PKS0235 + 164	5BZBJ0238 + 1636	LBL	185	172.8
1H0323 + 342	5BZUJ0324 + 3410	IBL	147	6.8
1ES0414 + 009	3HSPJ041652.5 + 010524	HBL	51	4.3
3C 120	5BZUJ0433 + 0521	LBL	176	4.3
PKS0506-61	5BZQJ0506-6109	LBL	59	4.0
TXS0506 + 056	5BZBJ0509 + 0541	IBL	82	13.4
GB6J0521 + 2113	3HSPJ052146.0 + 211251	HBL	81	110.4
5BZQJ0525-4557	5BZQJ0525-4557	LBL	51	7.2
PKS0528 + 134	5BZQJ0530 + 1331	LBL	134	25.2
RXSJ05439-5532	3HSPJ054357.2-553208	HBL	77	7.9
PKS0548-322	3HSPJ055040.6-321616	HBL	63	3.8
PKS0637-752	5BZQJ0635-7516	LBL	67	3.5
1ES0647 + 250	3HSPJ065046.5 + 250360	HBL	60	8.4
5BZBJ0700-6610	5BZBJ0700-6610	IBL	65	7.9
EXO0706.1 + 5913	3HSPJ071030.1 + 590821	HBL	64	5.3
S50716 + 714	5BZBJ0721 + 7120	IBL	329	69.6
3FGLJ0730.5-6606	3HSPJ073049.5-660219	HBL	64	24.6
GB6J0830 + 2410	5BZQJ0830 + 2410	LBL	104	48.9
S50836 + 71	5BZQJ0841 + 7053	LBL	77	5.5
GB6J0849 + 5108	5BZUJ0849 + 5108	LBL	56	20.9
OJ287	5BZBJ0854 + 2006	IBL	670	122.5
PKS0921-213	5BZUJ0923-2135	LBL	95	5.0
S40954 + 658	5BZBJ0958 + 6533	LBL	58	57.0
1ES1011 + 496	3HSPJ101504.1 + 492601	HBL	48	12.5
Mrk421	3HSPJ110427.3 + 381232	HBL	1163	107.4
PKS1130 + 009	5BZQJ1133 + 0040	LBL	58	13.9
GB6J1159 + 2914	5BZQJ1159 + 2914	LBL	75	17.3
MS1207.9 + 3945	3HSPJ121026.6 + 392908	HBL	411	6.5
1ES1218 + 304	3HSPJ122122.0 + 301037	HBL	113	12.5
ON231	5BZBJ1221 + 2813	IBL	120	82.0
PKS1222 + 216	5BZQJ1224 + 2122	IBL	113	10.5
3C 273	5BZQJ1229 + 0203	LBL	326	10.2
3HSP J123800 + 263553	3HSP J123800 + 263553	HBL	83	5.5
3C 279	5BZQJ1256-0547	LBL	421	11.4
PKS1406-076	5BZQJ1408-0752	LBL	82	8.6
PKS1424 + 240	5BZBJ1427 + 2348	LBL	85	16.3
PKS1424-41	5BZQJ1427-4206	LBL	63	7.4
H1426 + 428	3HSPJ142832.6 + 424021	HBL	179	3.8
PKS1502 + 106	5BZQJ1504 + 1029	LBL	105	8.9
PKS1510-08	5BZQJ1512-0905	IBL	267	6.8
1H1515 + 660	3HSPJ151747.6 + 652523	HBL	54	5.7
4FGLJ1544.3-0649	J154419.7-064916	HBL	50	34.7
PG1553 + 113	3HSPJ155543.1 + 111124	HBL	333	21.6
PKS1622-297	5BZUJ1626-2951	LBL	85	122.7
B31633 + 382	5BZQJ1635 + 3808	LBL	144	27.2
Mrk501	3HSPJ165352.2 + 394537	HBL	738	16.6
IZW187	3HSPJ172818.6 + 501311	HBL	160	13.1
PKS1730-130	5BZQJ1733-1304	LBL	93	14.0
S41749 + 701	5BZBJ1748 + 7005	IBL	57	12.2
S51803 + 784	5BZBJ1800 + 7828	LBL	72	6.0
3C 371	5BZBJ1806 + 6949	IBL	62	10.0
EXO1811.7 + 3143	3HSPJ181335.2 + 314418	HBL	57	172.0
2E1823.3 + 5649	5BZBJ1824 + 5651	LBL	70	7.5
4C + 56.27	5BZB J1824 + 5651	LBL	66	7.5
PKS1830-211	5BZQJ1833-2103	LBL	72	3.8

Table 1 – *continued*

Common or discovery name (1)	5BZB or 3HSP IAU denomination (2)	SED type (3)	Obs. with good spectra (4)	f_{max}/f_{min} @1 keV (5)
1ES1959 + 650	3HSPJ195959.8 + 650855	HBL	487	20.0
PKS2155-304	3HSPJ215852.1-301332	HBL	240	57.3
BLLac	5BZBJ2202 + 4216	IBL	545	206.6
CTA102	5BZQJ2232 + 1143	LBL	138	20.8
3C 454.3	5BZQJ2253 + 1608	LBL	414	24.4
1ES2344 + 514	3HSPJ234704.8 + 514218	HBL	184	10.3

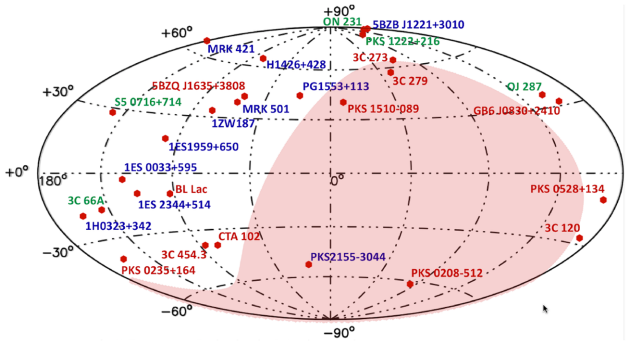

Figure 1. Hammer–Aitoff plot in Galactic coordinates showing the position of blazars that have been observed more than 100 times by Swift. The names of HBL sources appear in blue colour, while those of IBLs and LBLs are green and red, respectively. The light red area highlights the part of the sky south of the equator, illustrating how most of the blazars frequently observed by Swift are in the Northern hemisphere.

results presented here, should therefore, take into account of possible significant selection biases.

3 DATA PROCESSING

Data reduction and scientific analysis was performed using Swift_xrtproc, a software tool developed in cooperation between the Open Universe team and the ASI SSDC. This tool uses the XRT Data Analysis Software (XRTDAS[6]), and the spectral and imaging analysis tools XSPEC and XIMAGE, included in the HEASOFT package,[7] currently released as version V6.28.

3.1 Swift_xrtproc

Swift_xrtproc executes a complete data reduction, from XRT raw data to calibrated data products. The spectral and imaging data taken in PC or WT mode are analysed following standard procedures. The main steps that are performed on each Swift-XRT observation are:

(i) Automatic download of raw data and calibration files from one of the official Swift archives.

(ii) Generation of exposure maps and calibrated data products, for each snapshot and for the entire Swift observation, using the XRTPIPELINE task and adopting standard parameters and filtering criteria.

(iii) Source and background spectral files generation. The source counts are estimated in a circle of 20 pixels radius when no pile-up[8] is present. For the case of PC mode, the background is extracted in an annular region centred around the source with radius sufficiently large to avoid contamination from source photons. For the WT mode, the spectrum of the background is estimated from a deep observation taken from the XRT archive.

(iv) Pile-up correction. A verification of the source count-rate is carried out to determine whether the data is affected by pile-up. In case pile-up is present, the spectral data is extracted again excluding the central parts of the Point Spread Function, by taking counts in an annular region with inner radius chosen depending on the measured count-rate (Vaughan et al. 2006).

(v) Spectral fitting using the XSPEC package (Arnaud 1996) assuming a power-law and a log-parabola model.

(vi) Conversion of best-fit spectral data to $\nu f(\nu)$ units for SED plotting.

(vii) Photometric analysis using XIMAGE to estimate count-rates, or upper limits, in four energy bands: 0.3–1.0, 1.0–2.0, 2–10, and 0.3–10 keV, for data taken in PC readout mode.

(viii) Count-rate to X-ray flux conversion in the 0.5–10 and 2–10 keV energy bands and in $\nu f(\nu)$ units at the energies of 0.5, 1.5, and 4.5 keV.

(ix) Flux or upper limit estimation in $\nu f(\nu)$ units at 1 keV either from the best-fit spectrum or from the photometric data (in case the source is too weak for spectral fitting) suitable for light-curve generation and time-domain analysis.

3.1.1 *Spectral analysis*

We used the XSPEC spectral fitting package Version 12.11 to fit the X-ray data generated as described above to a power-law (equation 1) and to a log-parabola (equation 2) model, fixing the amount of absorbing column (NH) to the Galactic value.

$$N(E) = k * E^{-\Gamma} \quad (1)$$

where Γ is the photon index.

$$N(E) = k * E^{-(\alpha+\beta Log(E))} \quad (2)$$

where α is the photon spectral index at 1 keV and β is the curvature parameter. We chose these spectral shapes because they generally provide a good description of the X-ray spectra of blazars (e.g. Massaro et al. 2006) while keeping the number of free parameters to a minimum. Cash statistics (Cash 1979) was adopted for all spectral fits, grouping the data with the GRPPHA tool to include at least one count in each energy bin (Humphrey, Liu & Buote 2009).

[6]Developed under the responsibility of the ASI SSDC
[7]https://heasarc.gsfc.nasa.gov/docs/software/heasoft/

[8]Pile-up occurs when more than one photon hits the same pixel in a period shorter than the XRT-CCD readout time, typically 2.5 s in PC mode

Source name	RA (J2000.0) hh mm ss.d	Dec (J2000.0) dd mm ss	Phot index Photon index	Reduced chi2 red chisq pl	Alpha LP alpha_lp_with_err	Beta LP beta_lp_with_err	Reduced chi2 red chisq lp	Flux052 pl Flux 0.5-2	Flux210 pl Flux 2-10	Observation time mjd
3C273	12 29 06.5	+02 03 08	1.66±0.03	1.18	1.77±0.05	-0.23±0.08	1.1	3.3e-11±6.9e-13	6.7e-11±2.9e-12	53417.584
MRK501	16 53 52.2	+39 45 37	2.12±0.04	1.12	2.08±0.04	0.15±0.09	1.09	1e-10±2e-12	1e-10±6.9e-12	53426.042
MRK421	11 04 27.3	+38 12 32	2.7±0.01	1.01	2.69±0.02	0.05±0.04	1	8.8e-11±1.1e-12	3.9e-11±6.7e-13	53430.052
MRK421	11 04 27.3	+38 12 32	2.48±0.25	1.3	2.5±0.2	-1.07±0.8	0.95	2e-10±3.2e-11	1.2e-10±4.7e-11	53454.099
H1426+428	14 28 32.5	+42 40 19	2.01±0.06	1.21	2.04±0.08	-0.09±0.17	1.21	2.8e-11±7.8e-13	3.3e-11±2.6e-12	53460.004
H1426+428	14 28 32.5	+42 40 21	2.01±0.06	1.21	2.04±0.08	-0.09±0.17	1.21	2.8e-11±8.8e-13	3.4e-11±3.9e-12	53460.004
MRK421	11 04 27.3	+38 12 32	2.54±0.01	1.2	2.52±0.01	0.11±0.03	1.13	2.3e-10±1e-12	1.3e-10±1.1e-12	53460.043
1ES0033+595	00 35 52.6	+59 50 04	2.03±0.04	1.37	0.96±0.21	1.3±0.25	1.09	2.4e-11±8.1e-13	6.5e-11±2.1e-12	53461.032
MRK421	11 04 27.3	+38 12 32	2.4±0.01	1.24	2.36±0.01	0.16±0.03	1.05	3.6e-10±2.8e-12	2.5e-10±4.9e-12	53461.182
H1426+428	14 28 32.5	+42 40 19	2.02±0.03	0.93	2.03±0.04	-0.05±0.09	0.93	2.8e-11±5.5e-13	3.2e-11±1.9e-12	53462.952
H1426+428	14 28 32.5	+42 40 21	2.02±0.03	0.94	2.03±0.04	-0.05±0.1	0.94	2.8e-11±6.3e-13	3.3e-11±1.3e-12	53462.952
S50716+714	07 21 53.4	+71 20 35	2.16±0.2	1.31	2.69±0.65	-0.79±0.92	1.3	2.4e-12±2.4e-13	2.4e-12±6.8e-13	53462.979
S50716+714	07 21 53.4	+71 20 35	2.33±0.59	0.29	1.75±1.98	0.84±2.32	0.34	3e-12±1.2e-12	2.3e-12±1.3e-12	53464.715
1ES1959+650	19 59 59.5	+65 08 54	2.24±0.01	1.45	2.07±0.03	0.41±0.05	0.91	1.1e-10±1.4e-12	1.3e-10±1.6e-12	53479.046
1ES2344+514	23 47 04.9	+51 42 16	2.23±0.07	0.88	2.15±0.12	0.2±0.23	0.85	7.9e-12±2.6e-13	1e-11±6.5e-13	53479.052

Figure 2. A selection 15 lines from the on-line interactive and VO inter-operable table. The results of the analysis of all the spectral fits of the 65 blazars listed in Table 1 are accessible at https://openuniverse.asi.it/blazars/swift. A fits file including all the results is available at https://openuniverse.asi.it/OU4Blazars/oublazars_swift_spectra_v1.0.fits.gz.

3.1.2 Image analysis

All the XRT observations that were carried out in PC mode were also analysed using the XIMAGE (V4.5.1) X-ray image analysis package.[9] The procedure used is equivalent to that implemented in the Swift_deepsky tool (Giommi et al. 2019, 2020c), which performs a photometric flux estimation using X-ray data in four energy bands: 0.3–10 keV (full band), 0.3–1.0 keV (soft band), 1.0–2.0 keV (medium band), and 2.0–10.0 keV (hard band). The image background was measured using the XIMAGE/background command, and source counts were obtained using the XIMAGE/SOSTA tool centring on the target and counting events in boxes whose size includes 80 per cent of the source flux (see Giommi et al. 2019, for more details). Spectral slopes were also estimated from the hardness ratio, defined as the ratio between the counts in the hard and soft bands. Count-rates (or upper limits) were converted to X-ray fluxes assuming NH equal to the Galactic value, and a power-law spectrum with spectral index equal to the value estimated from the XSPEC spectral analysis when available or from the hardness ratio. When no spectral slope estimation was possible the spectral index was assumed to be equal to 1.8. Fluxes in $\nu f(\nu)$ units, suitable for SED plotting, were calculated at the reference energies of 0.5, 1.5, and 4.5 keV. Finally, a second spectral slope estimation was obtained via a least square linear fit to the 0.5, 1.5, and 4.5 keV $\nu f(\nu)$ fluxes.

4 RESULTS

We processed a total of 31 068 Swift-XRT observations or individual snapshots of the 65 blazars listed in Table 1. This led to the generation of 29 050 X-ray spectra, 21 141 photometric flux estimations, and 206 upper limits.

4.1 Best-fit parameters and fluxes

The results of the XSPEC spectral fits for every spectrum including at least 20 source counts, are reported in the on-line interactive table available at https://openuniverse.asi.it/blazars/swift, (see Fig. 2). Column 1 gives the source name, columns 2, and 3 the J2000.0 Right ascension and Declination, columns 4 and 5 give the best-fit photon spectral index with error and the reduced χ^2, columns 6, 7, and 8 give the α, β best-fit parameter and χ^2 for the log-parabola model, column 9 and 10 give the observed flux in the 0.5–2.0 and 2–10 keV bands, column 11 gives the observation time. The complete set of results are also available as a fits file.[10]

4.1.1 Power-law Vs Log-parabola models

Our results confirm with large statistics that the log-parabola model generally fits best the X-ray spectral shape of HBL blazars, while LBL sources are usually best fit by a simple power-law. IBL blazars often show more complex spectra, as in these cases the steep end of the synchrotron component merges into the much flatter inverse Compton component in the X-ray band. As a particular example of HBL blazar, Fig. 3 plots the distribution of the best-fit Cash statistics divided by the number of degrees of freedom (Cstat/degrees of freedom) values for the power-law and log-parabola fits of Mrk421. The sharper and lower value peaking red histogram for the case

[9] https://heasarc.gsfc.nasa.gov/xanadu/ximage/

[10] https://openuniverse.asi.it/OU4Blazars/oublazars_swift_spectra_v1.0.fits.gz whose structure is described in Table 2

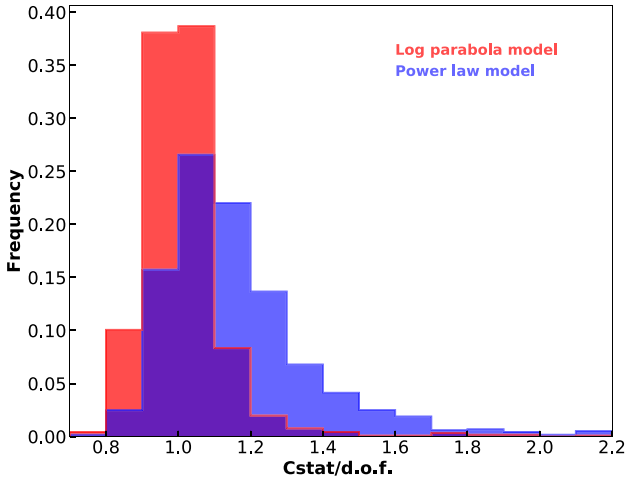

Figure 3. The normalised distributions of best-fit Cstat statistics divided by the number of degrees of freedom (Cstat/degrees of freedom) for the power-law and log-parabola models for the case of the blazar Mrk 421. The log-parabola model gives systematically lower Cstat/degrees of freedom values, implying that this model is clearly a better representation of the data for this blazar.

of log-parabola demonstrates that this spectral model is a better representation than a simple power-law. Similar results are obtained for most blazars of the HBL type. The X-ray spectra of IBL blazars are mostly characterized by a steep power-law spectrum since the XRT band-pass in these objects covers the end of the synchrotron tail and occasionally show the onset of the second SED hard component. The X-ray spectrum of LBL blazars is well represented by a simple power-law spectrum with a flat slope, with average value of $\langle\Gamma\rangle = 1.46$. In some cases, however, (see e.g. the SED of 3C 273 and CTA102 in Fig. 4) there is some evidence for a flattening toward the high-energy end of the XRT energy window.

The spectral shapes described above can also be noted from a simple visual inspection of the SEDs of Figs 4, 5, and 6 and those available in the on-line table at https://openuniverse.asi.it/blazars/swift.

4.2 Imaging analysis

The results of the imaging analysis, including count-rates, fluxes in the 0.5–10.0, and 2–10 keV bands, $\nu f(\nu)$ fluxes at 0.5, 1.0, 1.5, and 4.5 keV, as well as two estimates of the spectral index, are given in the fits-formatted file mentioned above and described in Table 2.

4.3 Spectral Energy Distributions

The best-fit spectral data and the X-ray fluxes estimated from the imaging analysis have been combined with archival multifrequency data retrieved using the VOU-Blazars software (Chang et al. 2020) to build the radio to γ-ray SED of each object in the sample. The VOU-Blazars tool provides access to data from over 70 catalogues and spectral databases covering the entire electromagnetic spectrum. Figs 4, 5, and 6 give examples of SEDs of representative blazars of the LBL, IBL, and HBL class. The SED of all the blazars in the sample are available on-line at https://openuniverse.asi.it/blazars/swift. Grey points represent archival data, green symbols are the XSPEC best-fit spectral data, red points are from the XIMAGE/SOSTA measurements, and the light yellow points are the 1 keV $\nu f(\nu)$ fluxes calculated as described in Section 4.4. Note that the red points are not present in a

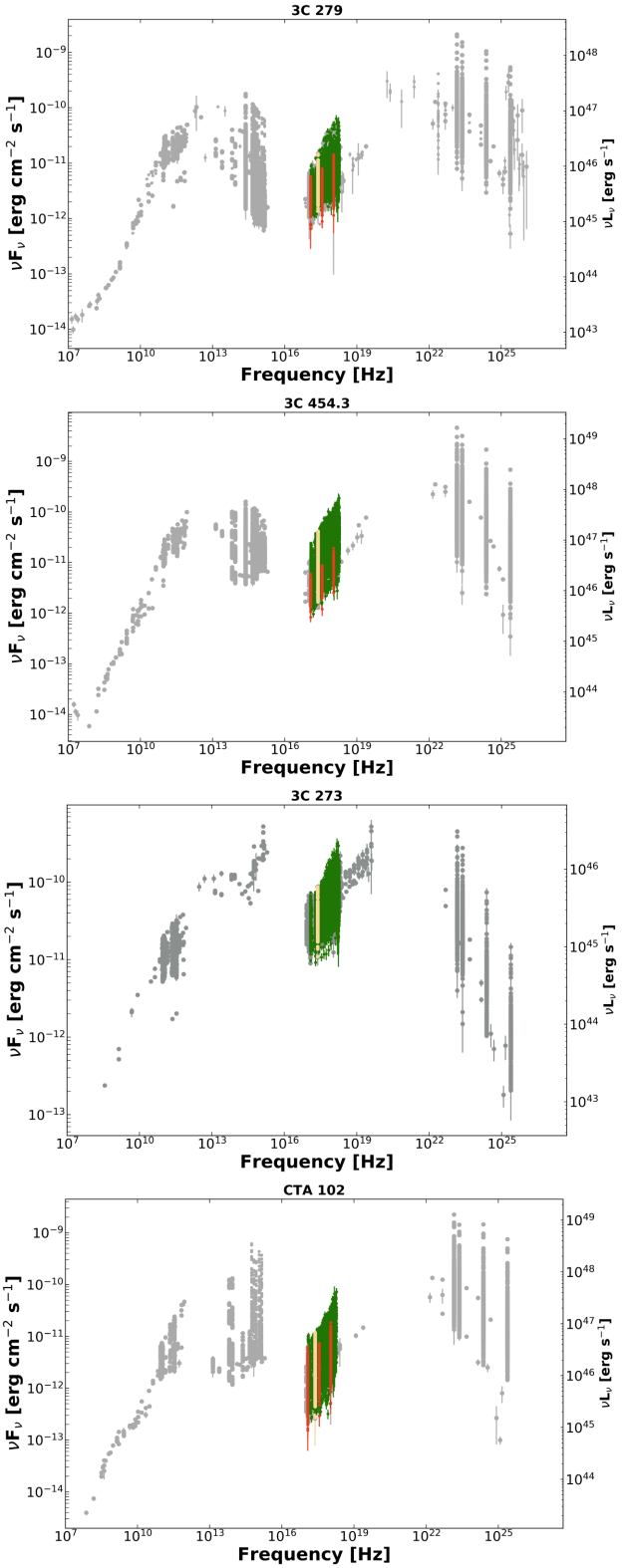

Figure 4. SED of representative LBL blazars showing the XSPEC best-fit spectra (WT and PC mode, green points), the results of the XIMAGE photometric analysis (only PC mode, red points), the overall 1 keV light-curve points (light yellow points) and archival multifrequency data from VOU-Blazars (grey points).

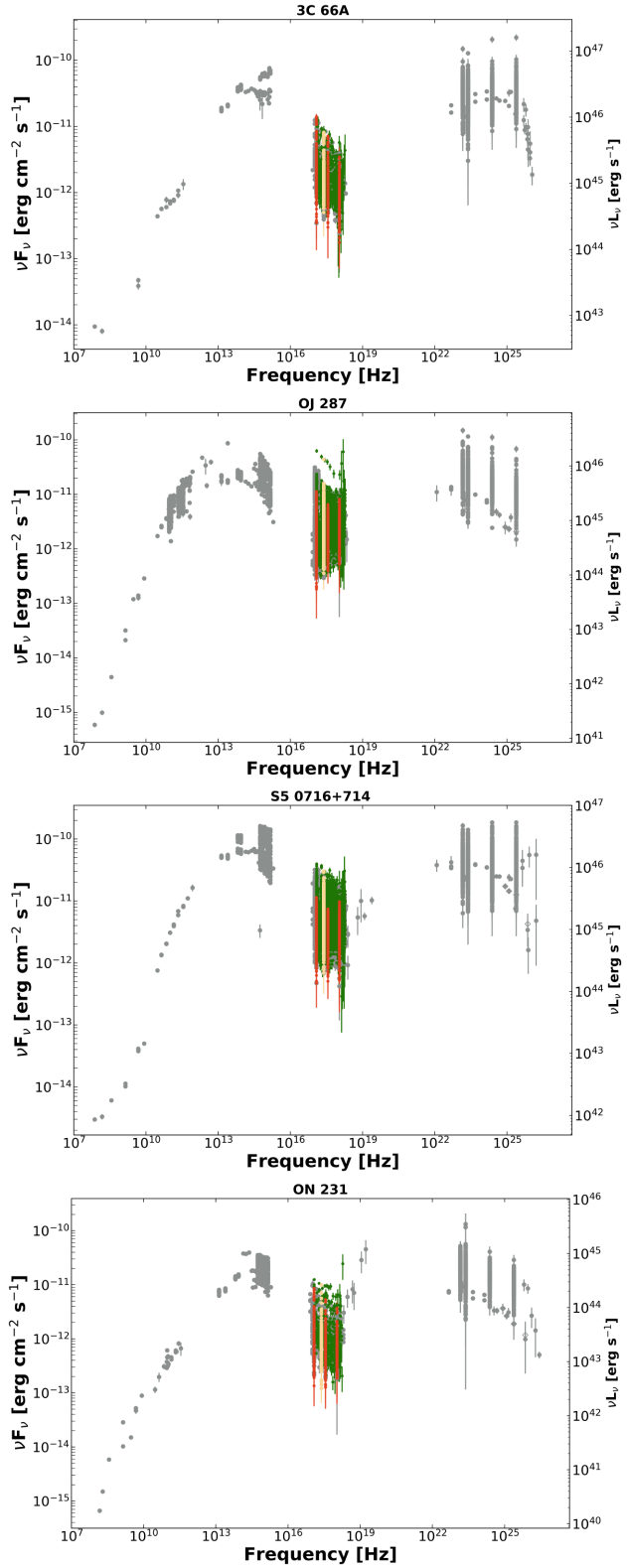

Figure 5. SED of representative IBL blazars showing the XSPEC best-fit spectra (WT and PC mode, green points), the results of the XIMAGE photometric analysis (only PC mode, red points), the overall 1keV light-curve points (light yellow points) and archival mult-frequency data from VOU-Blazars (grey points).

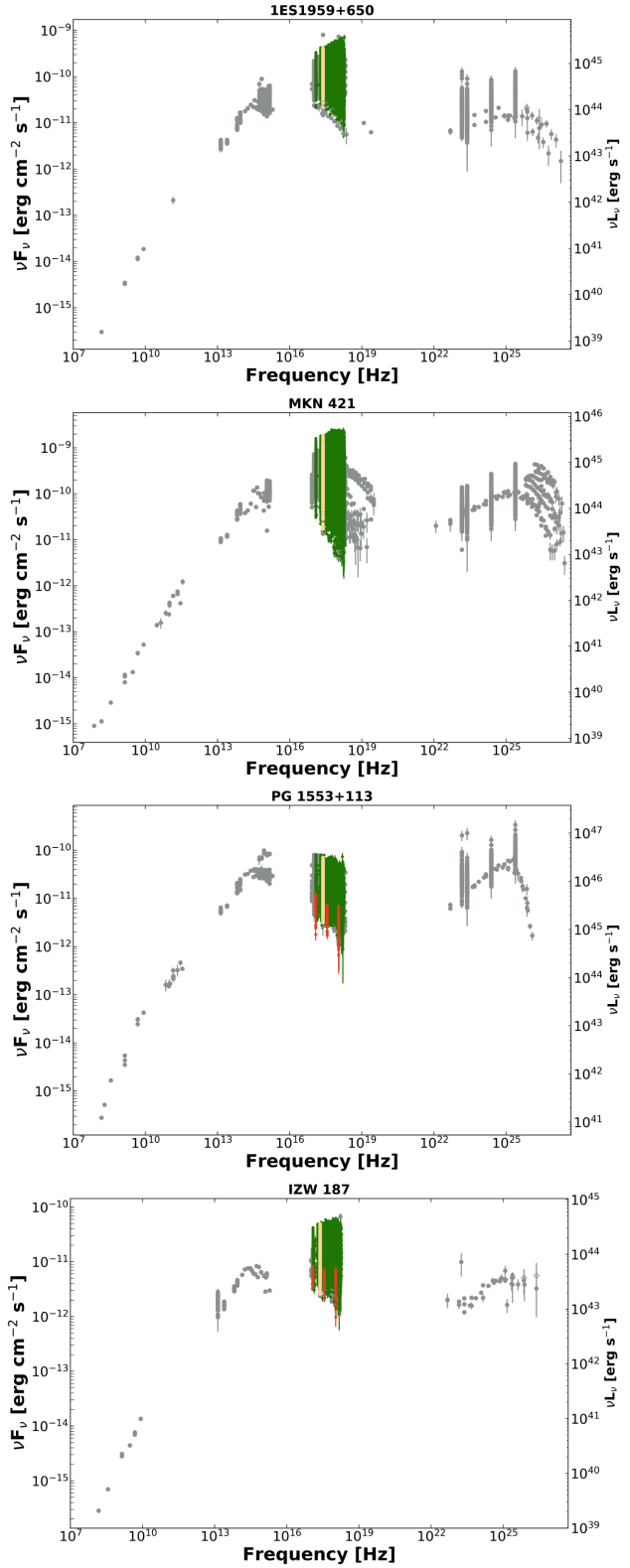

Figure 6. SED of representative HBL blazars showing the XSPEC best-fit spectra (WT and PC mode, green points), the results of the XIMAGE photometric analysis (only PC mode, red points), the overall 1 keV light-curve points (light yellow points) and archival multifrequency data from VOU-Blazars (grey points).

Table 2. Content of the FITS file including the results of the spectral fits and of the image analysis.

Column	Format	Units	Description
Blazar name	15A		Blazar name
R.A.	D	deg	Right Ascension in degrees (J2000.0 epoch)
Dec.	D	deg	Declination in degrees (J2000.0 epoch)
MJD	D	days	Modified Julian Day of observation start time
Obs_time	D	s	observation start time in units yyyy.ff where ff is the fraction of year
Sequence	A		Swift observation ID
Flux2_10-PL	D	erg cm^{-2} s^{-1}	2–10 keV flux from best-fit power-law model
Flux2_10-PL_error	D	erg cm^{-2} s^{-1}	1 sigma error on Flux2_10-PL
Flux05_2-PL	D	erg cm^{-2} s^{-1}	0.5–2.0 keV flux from best-fit power-law model
Flux05_2-PL_error	D	erg cm^{-2} s^{-1}	1 sigma error on Flux05_2-PL
Flux03_3-PL	D	erg cm^{-2} s^{-1}	0.3–3.0 keV flux from best-fit power-law model
Flux03_3-PL_error	D	erg cm^{-2} s^{-1}	1 sigma error on Flux03_3-PL
χ^2_r-PL	D		reduced χ^2 for power-law model
Degrees of freedom-PL	D		degrees of freedom for power-law model
χ^2_r-LP	D		reduced χ^2 for log-parabola model
Degrees of freedom-LP	D		degrees of freedom for log-parabola model
Photon_index	D		best-fit photon index for power-law fit
Photon_index_error	D		error on best-fit photon index for power-law fit
Normalization-PL	D		best-fit power-law normalization
Normalization-PL_error	D		error on best-fit power-law normalization
α	D		best-fit α parameter for log-parabola fit
α_error	D		error on α parameter for log-parabola fit
β	D		best-fit β parameter for log-parabola fit
β_error	D		error on β parameter for log-parabola fit
Normalization-LP	D		best-fit log-parabola normalization
Normalization-LP_error	D		error on best-fit log-parabola normalization
Snapshot	3A		swift snapshot number 'TOT' for full observation
νf(ν) @1.0 keV	D	erg cm^{-2} s^{-1}	νf(ν) flux at 1.0 keV
νf(ν) @1.0 keV_error	D	erg cm^{-2} s^{-1}	error νf(ν) flux at 1.0 keV
Datamode	2A		XRT data readout mode: PC or WT
I-νf(ν) @0.5 keV	D	erg cm^{-2} s^{-1}	νf(ν) flux at 0.5 keV from image analysis
I-νf(ν) @0.5 keV_error	D	erg cm^{-2} s^{-1}	error νf(ν) flux at 0.5 keV
I-νf(ν) @1 keV	D	erg cm^{-2} s^{-1}	νf(ν) flux at 1.0 keV from image analysis
I-νf(ν) @1 keV_error	D	erg cm^{-2} s^{-1}	error νf(ν) flux at 1.0 keV
I-νf(ν) @1.5 keV	D	erg cm^{-2} s^{-1}	νf(ν) flux at 1.5 keV from image analysis
I-νf(ν) @1.5 keV_error	D	erg cm^{-2} s^{-1}	error νf(ν) flux at 1.5 keV
I-νf(ν) @4.5 keV	D	erg cm^{-2} s^{-1}	νf(ν) flux at 4.5 keV from image analysis
I-νf(ν) @4.5 keV_error	D	erg cm^{-2} s^{-1}	error νf(ν) flux at 4.5 keV
I-Flux0510	D	erg cm^{-2} s^{-1}	0.5–10.0 keV flux from image analysis
I-Flux0510_error	D	erg cm^{-2} s^{-1}	error on 0.5–10.0 keV flux from image analysis
I-Flux210	D	erg cm^{-2} s^{-1}	2.0–10.0 keV flux from image analysis
I-Flux210_error	D	erg cm^{-2} s^{-1}	error on 2.0–10.0 keV flux from image analysis
I-Photon_index	D		power law photon index fit from hardness ratio
I-Photon_index_error	D		error on photon index for power-law fit
SED-Photon_index	D		photon index for power-law fit estimated from a fit to I-νf(ν) @0.5keV, I-νf(ν) @1.5keV and I-νf(ν) @4.5keV
SED-Photon_index_error	D		error on photon index
SED-Photon_index_error	D		error on photon index for power-law fit
CR(0.3-10 keV)	D	cts s^{-1}	count-rate in 0.3–10.0 keV energy band
CR(0.3-10 keV)_error	D	cts s^{-1}	error on count-rate in 0.3–10.0 keV energy band
O-νf(ν) @1 keV	D	erg cm^{-2} s^{-1}	overall νf(ν) flux at 1.0 keV for light curves
O-νf(ν) @1 keV_error	D	erg cm^{-2} s^{-1}	error on overall νf(ν) flux at 1.0 keV
Upper limit flag	2A		flag set to 'UL' if the count rate is a 3σ limit, blank otherwise

high-intensity states when the WT readout mode was used, reflecting the fact that imaging analysis was only performed when the XRT was operated in PC mode.

4.3.1 *Synchrotron peak energy (ν_{peak})*

Reliable values of $\nu_{\rm peak}$ can be estimated directly from the X-ray spectrum in all sources where the log-parabola model is a good fit

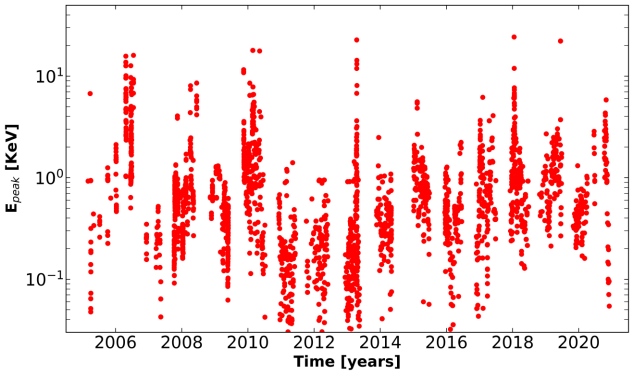

Figure 7. The remarkable changes of the synchrotron peak energy in the SED of Mrk 421 over a period of 16 years of Swift monitoring of this object.

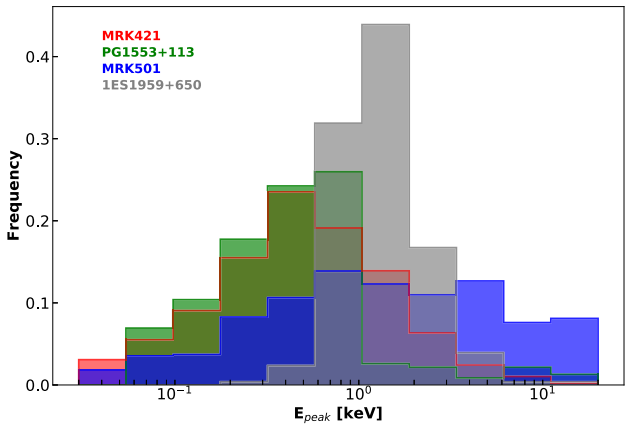

Figure 8. The distribution of the synchrotron peak energy observed in bright HBL blazars as examples representing the class. Large $\nu_{\rm peak}$ variations are commonly observed. Most of the other HBL sources in our sample show similar $\nu_{\rm peak}$ variations.

to the data and $\nu_{\rm peak}$ is located inside or close to the XRT band-pass. From Massaro et al. (2006) we have

$$\nu_{\rm peak} = 10^{(2-\alpha)/2\beta} \quad (3)$$

where α and β are the parameters of equation 2. We have calculated $\nu_{\rm peak}$ in all cases where well estimated values of α and β could be obtained and equation 3 gives values that are close or within the Swift-XRT X-ray band. We found that large variations of this parameter are detected in many objects. As an example of this behaviour Fig. 7 plots $\nu_{\rm peak}$ as a function of time for the case of Mrk421, the object most frequently observed in the sample, showing frequent large changes spanning over two orders of magnitude, from below 0.1 to over 20 keV. Large $\nu_{\rm peak}$ changes are common in most HBL blazars, as illustrated in Fig. 8 which plots the $\nu_{\rm peak}$ distribution of Mrk421 together with three other representative sources. Values close to the low and high-energy ends of Fig. 8 should be taken with caution (and perhaps treated as limits, see e.g. Kapanadze et al. 2016a, 2020) since they are at the edge of the XRT energy range. However, the frequency of occurrence is low and the impact on the overall shape of the distribution is limited.

4.4 Time domain data

Detailed temporal studies of the X-ray emission in blazars is beyond the scope of this paper. In the following, we limit ourselves to present the 1 keV light curves of all the blazars in the sample and briefly comment on the long-term variability and flux variations between neighbouring snapshot, based on visual inspection of the data. A comprehensive study of blazars temporal behaviour based on the data presented here will be the subject of a future publication.

The light curves presented in this paper are based on 1 keV ($\nu f(\nu)$) fluxes, calculated as the best-fit value (and statistical error) of the power-law normalization, multiplied by 1.6×10^{-9}, to convert from XSPEC units to erg cm^{-2} s^{-1}, or converting to 1 keV the XIMAGE count-rate estimation in the soft band, when less than 20 source counts were detected, or 3σ upper limits estimated with the XIMAGE/SOSTA command in case of non-detection.

4.4.1 Long-term light curves

1 KeV $\nu f(\nu)$ light curves covering the period November 2004 to the end of 2020 of all the sources in the sample can be accessed on-line at https://openuniverse.asi.it/blazars/swift/. Figs 9, 10, and 11 show examples of light curves of five representative LBL, IBL, and HBL blazars, respectively. Blue points represent fluxes averaged over the entire observation, red points correspond to single snapshots. Large luminosity variability on different amplitudes and timescales, ranging from factor of a few to over a factor 200, is present in all sources. The ratio between the maximum and minimum observed flux in each source is listed in column (5) of Table 1.

Light curves based on integrated XRT fluxes in the 0.5–2.0, 0.3–3.0, 0.5–10, and 2–10 keV bands, or $\nu f(\nu)$ fluxes at the energy of 0.5, 1.5, 4.5 keV, can be produced using the data provided in the fits file described in Table 2.

4.4.2 Harder-when-brighter and softer-when-brighter behaviour

Spectral changes correlated with intensity variations in blazars were first noticed in early EXOSAT X-ray observations of PKS2155-304 (Morini et al. 1986) and of Mrk421 (George, Warwick & Bromage 1988). A study conducted on a sample of 36 BL Lacs showed that this behaviour is a common feature of BL Lacs objects (Giommi et al. 1990). In the following, we investigate these correlations in our sample, which includes all types of blazars and a much larger number of observations.

The upper panel of Fig. 12 plots the best-fit power-law spectral index as a function of X-ray flux for the source Mrk501. A clear trend is present, with steep spectral slopes ($\Gamma \gtrsim 2.5$) being observed during low flux periods and much harder ($\Gamma \sim 1.5$) values during high-intensity states. This harder-when-brighter behaviour is common to the HBL sources in our sample as can also be noticed in the SEDs of Fig. 6.

A case of the opposite (softer-when-brighter) trend is shown in the middle panel of Fig. 12 for the case of the IBL blazar OJ287. In this intermediate ν_{peak} situation the X-ray flux strongly increases when ν_{peak} reaches values larger than $\approx 10^{14.5}$ Hz and the steep tail of the synchrotron SED component enters the X-ray band. When ν_{peak} is instead located at lower frequencies, the synchrotron component does not reach X-ray energies and the flux in the X-ray band is only due to the hard inverse Compton component.

The lower part of Fig. 12 illustrates the case of the LBL object 3C 273, which shows an apparent harder-when-brighter behaviour. This is likely not due to an intrinsic hardening of the inverse Compton emission from the jet but rather to a changing mix of different components. This is because during high intensity states the flat radiation from the jet dominates the steeper X-ray emission from the accretion on to the supermassive black hole (e.g. Grandi & Palumbo 2004).

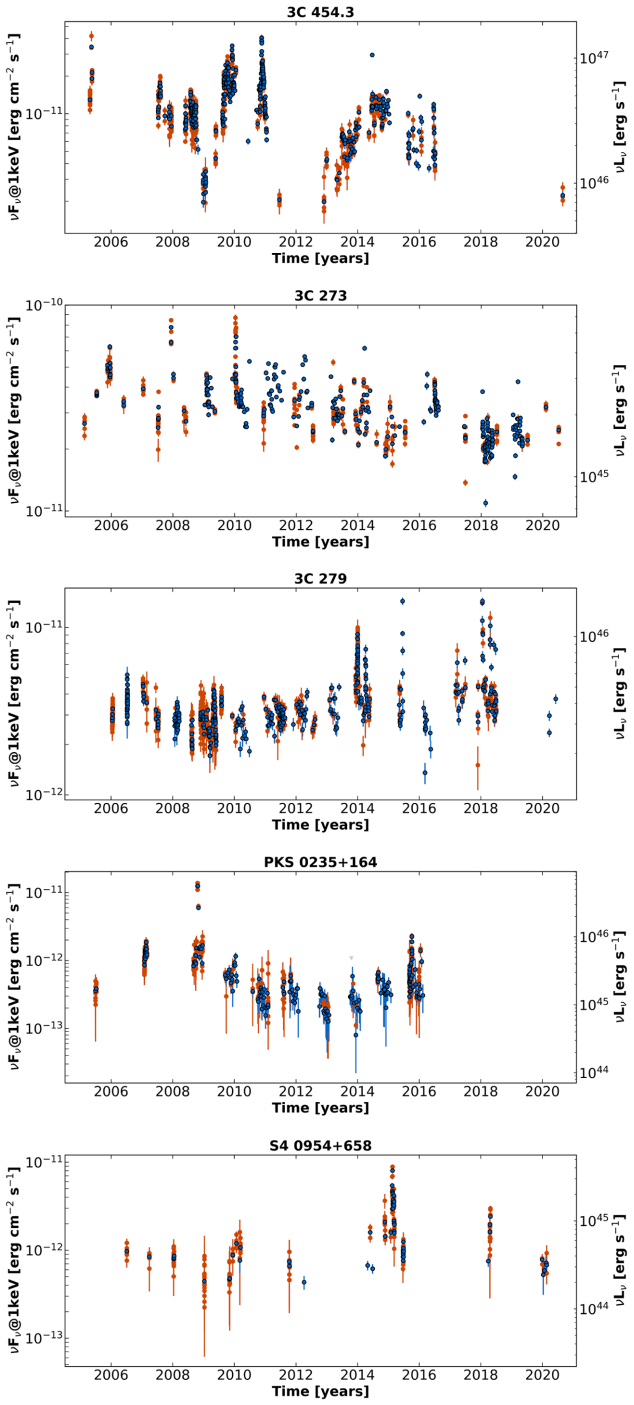

Figure 9. The 1 keV light curves of LBL blazars: 3C 453.4, 3C 273, 3C 279, PKS0235+164, and S4 0954 + 658.

4.4.3 Rapid variability

Large X-ray luminosity variability on a variety of timescales in blazars is common and amply documented in the literature (e.g. Giommi et al. 1990; Kapanadze et al. 2016b, 2017, 2018a, b, c, d,

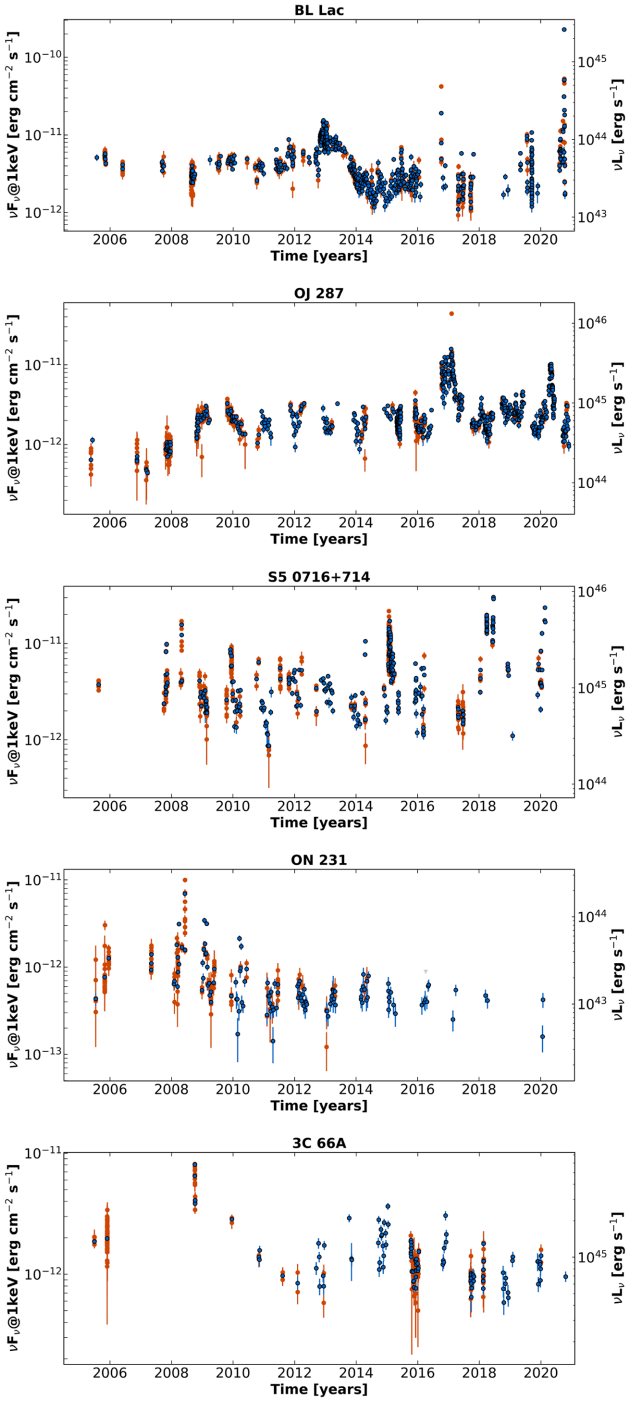

Figure 10. The 1 keV light curves of IBL blazars: BL Lacertae, OJ 287, S5 0716 + 714, ON 231, and 3C 66A.

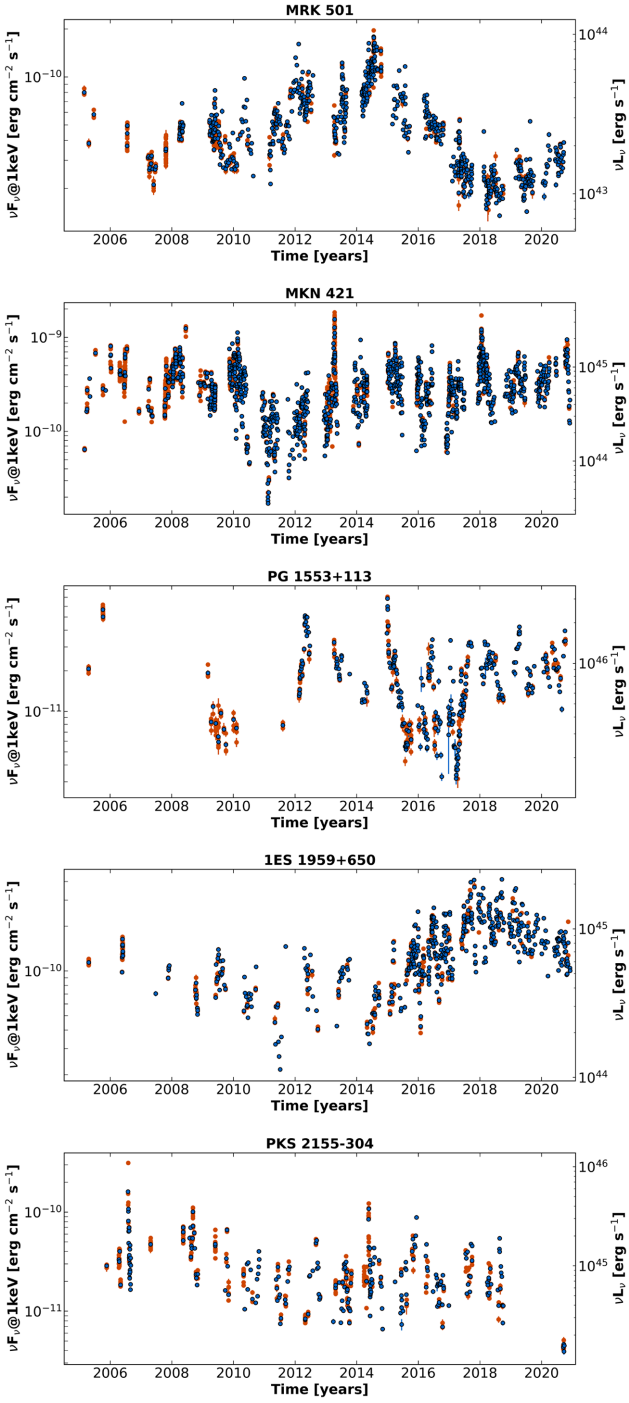

Figure 11. The 1 keV light curves of HBL blazars: Mrk 501, Mrk 421, PG1553+113, 1ES1959 + 650, and PKS2155-304.

2020; Wang et al. 2018, and references therein). We searched for large amplitude ($\gtrsim$ 50 per cent) variability on timescales of the order of one or a few hours by comparing the flux observed during contiguous or neighbouring snapshots, which are typically separated by one Swift orbit, or $\sim$ 1.5 h. Large luminosity variations on these timescales are rarely observed in our sample. This may reflect the fact that this type of variations are intrinsically rare in blazars, but it could also be due to limited sampling or observing strategy, as in many cases the observations consisted of single snapshot exposures. The list of the thirteen objects where rapid variability has been noticed is given in Table 3 where column 1 gives the blazar name, column 2 gives the Swift Observation ID, column 3 the time in MJD units, column 4 the time difference between the snapshots where the variability was observed, and column 5 gives the ratio between the flux measured in the last snapshot and that of the first snapshot.

5 DISCUSSION

The analysis presented in the previous sections shows that long-term large amplitude X-ray variability is present in the data of all blazars

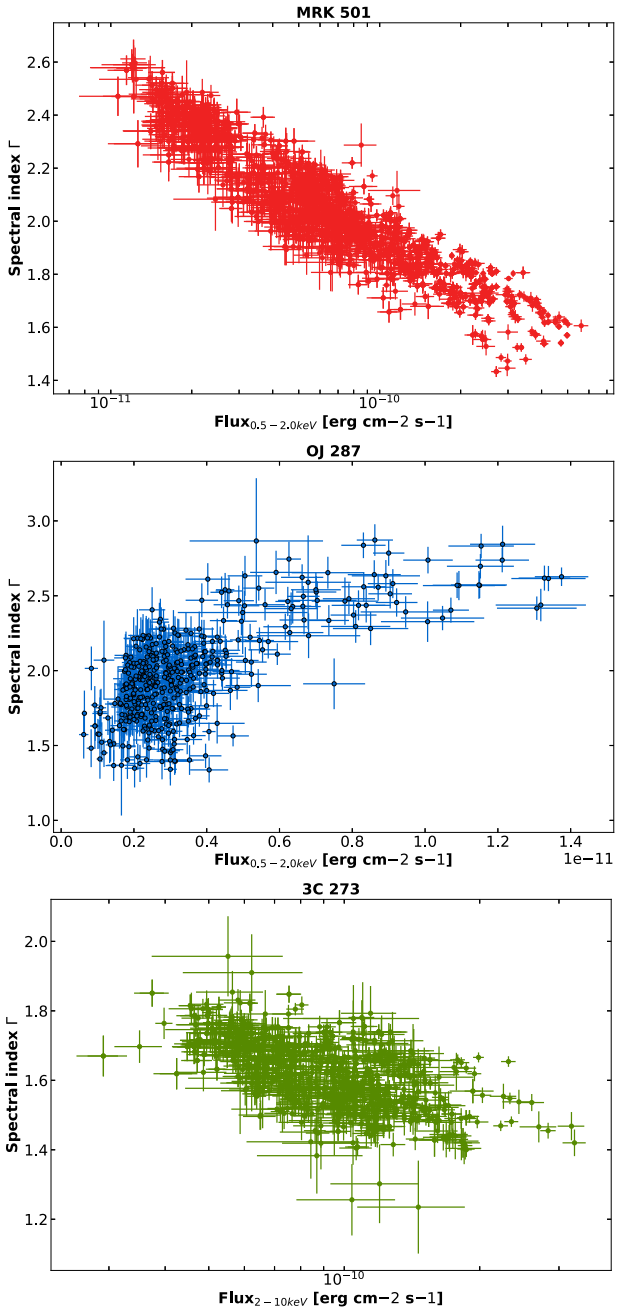

Figure 12. Plot of the power-law spectral slope versus X-ray flux for the HBL blazar Mrk501 (upper panel), for the IBL object OJ287 (middle panel), and 3C 273 (lower panel) illustrating the various cases of harder-when-brighter, and softer-when-brighter behaviour in blazar spectral variability.

of the sample on a variety of timescales (see Table 1 and the light curves of Figs 11, 10, and 9).

No obvious periodicities or regularities can be seen from a visual inspection of the light curve of any object. However, these results cannot be considered an unbiased view of the long-term behaviour of blazars since X-ray sources that are frequently observed by Swift are often pointed as Target of Opportunity triggered by flaring activity discovered in other parts of the electromagnetic spectrum. Nevertheless, the results presented here provide a new rich dataset that is very useful to study the observational properties of blazars and constrain physical models in the energy and time domain. In the following, we make some initial considerations on blazars properties that are not significantly affected by the selection biases of the sample.

Table 3. Blazars where flux variability was observed between consecutive or neighbouring snapshots.

Name	Obsid	Date (MJD)	Δ T (Ks)	f_{f2}/f_{f1}
(1)	(2)	(3)	(4)	(5)
1H0323 + 342	00035372001	53922.8	5	2.4
1H0323 + 342	00035630002	53926.6	6	1.7
1ES0414 + 009	00081691001	57353.9	6	0.5
TXS0506 + 056	00083368006	58031.7	5	0.3
3C 120	00037594042	56934.2	5	1.5
OJ287	00033756119	57792.3	11	0.3
OJ231	00031219001	54624.9	15	4.1
PKS0548-322	00044002081	58370.9	5	0.3
Mrk421	00030352011	53905.4	5	2.9
PG1553 + 113	00031368076	57021.8	5	0.7
EXO1811.7 + 3143	00013748001	59125.5	4	1.5
1ES1959 + 650	00034588249	59164.9	1	1.7
PKS2155-304	00030795001	53946.1	75	2.7
BLLac	00034748002	57668.3	5	0.2

5.1 X-ray emission in blazars of different types: HBLs versus IBLs versus LBLs

Our sample includes 24 HBL, 12 IBL, and 29 LBL blazars. The X-ray band is particularly important in the energy spectrum blazars of all types, as the X-ray flux of HBL sources is entirely due to synchrotron emission, while in IBL objects the end of the synchrotron tail often merges with the second (inverse Compton or other) high-energy component. In LBL sources, the X-ray flux instead maps the beginning of the second SED bump. Different spectral shapes, variability properties, and probably also time lags between the soft and hard X-ray band, are to be expected in blazars of different types.

The location and variability properties of ν_{peak} provide crucial information about the physical conditions in blazars jets. Among the important physical parameter that can be constrained are the maximum particles energy, the acceleration, and cooling times, the size of the emitting region, and the distribution of the particles responsible for the non-thermal radiation that we observe. The results obtained with our large data-set on this important parameter can be summarized as follows:

(i) The SEDs of the 65 objects in our sample, some of which are shown in Figs 4, 5, 6, confirm with large statistics that ν_{peak} in blazars ranges from $\sim 10^{12}$ Hz, to well over 10^{18} Hz.

(ii) The position of ν_{peak} is not constant in time, as noticed over twenty years ago in the *BeppoSAX* data of Mrk501 and 1ES2344 + 514 (Pian et al. 1998; Giommi, Padovani & Perlman 2000), and more recently studied in detail in some objects (e.g. Kapanadze et al. 2018b, 2020). Our results show that frequent and large variations of ν_{peak}, spanning a range of well over a factor 100 in some objects, is a very common, likely ubiquitous, feature of HBLs. As an example, Fig. 7 illustrates how frequently ν_{peak} changes in time and amplitude in Mrk421, the blazar most frequently observed by Swift. The SEDs plotted in Fig 6, and those available on-line show that this phenomenon is present in most HBLs of the sample. Fig. 8 shows the distribution of ν_{peak} in four representative HBL blazars, where we can see that blazars of this type spend a significant fraction of the time with ν_{peak} values that are more than a factor

5 away from the average value. Note that these histograms may be a partially distorted representation of the intrinsic probability distributions because of the selection biases of the sample. This is because ToO observations tend to follow large $\nu_{\rm peak}$ values during flares, rather than quiet periods. In addition, the relatively narrow band-pass of XRT limits the range over which $\nu_{\rm peak}$ can be safely estimated to ∼0.5 and 8–10 keV.

(iii) Variations of $\nu_{\rm peak}$ in IBL sources are difficult to detect with XRT data alone since $\nu_{\rm peak}$ in these objects is located outside the X-ray band. Despite that, Giommi et al. (2008) combining Swift UVOT and XRT data, found evidence for $\nu_{\rm peak}$ variations in the IBL blazar S50716 + 714. Harder-when-brighter trends has been found in the infrared and optical part of the spectrum of the same object by Xiong et al. (2020) and Morokuma et al. (2020), suggesting that large $\nu_{\rm peak}$ variations should be present in IBL blazars as well.

(iv) Variations of the SED peak frequency in LBLs are also hard to observe because of the lack of multi-epoch observations in the far-infrared, where $\nu_{\rm peak}$ is located in these sources. However, at least in the cases of CTA 102, 3C 279, and 3C 454.3 (see Fig. 4.), where large intensity variations in the IR/optical/UV and X-ray band have been detected, no significant spectral changes have been detected, consistently with no evidence for a large increase of $\nu_{\rm peak}$ in LBLs. An optical-infrared monitoring of γ-ray emitting blazars of different types (Bonning et al. 2012) detected a tendency for FSRQs (all of which are of the LBL type) to become bluer when fainter. This apparent hardening was interpreted as due to the blue accretion disk emission becoming increasing dominant during faint states of the jet component. When the sources were found in a bright state the spectrum tended to become redder (steeper), implying that $\nu_{\rm peak}$ in these sources was not moving from the far-IR to energies close to the optical band.

(v) Most of the X-ray flux enhancements in HBL sources is due to the effects of spectral hardening, rather than to an overall flux increase at all energies. This effect is larger when $\nu_{\rm peak}$ is located in the very soft X-ray band. In this situation, a small increase of this parameter flattens the X-ray spectrum inducing large flux increases. On the other hand, when $\nu_{\rm peak}$ reaches values that are larger than the energy band where the flux is measured, no significant flux increase is often observed. This behaviour may be due to a $\nu_{\rm peak}$ increase without an associated increase in the normalization of the spectrum, or to the onset of a second hard component related to a different emitting region. This second hypothesis was first considered by Giommi et al. (2000), who interpreted the $\nu_{\rm peak}$ shift in 1ES2344 + 514 as the result of a different component emerging at high energies.

Most values of $\nu_{\rm peak}$ reported in the literature are estimated under one of these circumstances: (a) on the basis of a single X-ray observation, (b) based on the average value of several X-ray measurements, or (c) on sparse archival X-ray data taken at different epochs. In all cases, the value of $\nu_{\rm peak}$ may be biased for the following reasons: when a blazar has been observed many times, the observations are often the result of monitoring campaigns carried out in response to the announcement of a large flare or of a high state of the object. Since there is a strong correlation between source intensity and $\nu_{\rm peak}$ (in most cases higher $\nu_{\rm peak}$ when the source brightens, e.g. Kapanadze et al. 2018b, 2020) the average flux and the corresponding $\nu_{\rm peak}$ will be biased towards high values. When instead a blazar has only one X-ray observation (e.g. objects discovered in the RASS survey, Voges et al. (1999), and never observed afterwards), the value of $\nu_{\rm peak}$ is a random draw from the (intrinsic, perhaps time dependent) $\nu_{\rm peak}$ distribution similar to those shown in Fig. 8. If this single draw is a low value that corresponds to a flux below the X-ray sensitivity limit, the blazar is not even discovered. Those above the X-ray limit but close to it, as in many real cases, will have a value of $\nu_{\rm peak}$ that is biased towards high values.

Some of the so-called extreme blazars (Biteau et al. 2020), might therefore, not be really extreme sources, but objects that spend most of their time with moderately high $\nu_{\rm peak}$ values and happened to have been discovered in a high state.

5.2 Unexpected findings and future samples

The existence of transient blazars was not known until the detection of 4FGLJ1544.3-0649 (Sahakyan & Giommi 2021), one of the objects in our sample. This object remained hidden in the archives as one of the many anonymous radio sources with no associated high-energy emission, until May 2017 when Ciprini et al. (2017) reported the emergence of a new Fermi-LAT transient source, triggering observations at other frequencies. These new data led to the identification of a new blazar, which for a few months became one of the brightest objects of this type in the X-ray and γ-ray bands.

The unexpected existence of transient blazars could complicate or even modify our perception of this type of sources if 4FGLJ1544.3-0649 does not represent an isolated case but rather the tip of the iceberg of a previously unnoticed phenomenon. It is likely that similar sources are present in the existing archival data or will be found in future sensitive observations.

The SRG/eROSITA (Merloni et al. 2012; Merloni, Nandra & Predehl 2020) XRT is conducting an all-sky X-ray survey with good sensitivity, repeated at different epochs. This survey will have a deep impact on blazar science with the discovery of a few thousand new objects with multiple detections, especially of those located near the ecliptic poles, thus mitigating or largely removing the biases described above. This extremely valuable data-set, alongside the science archives of the forthcoming and previous space missions and ground based observatories, constitute a colossal, ever growing, reservoir of information. It is clear that it is not possible to efficiently convert this enormous potential into knowledge following a traditional approach based on the analysis of low or intermediate level data from every instrument, each requiring specific expertise. Only the easily-accessible/transparent availability of science-ready data products will enable us to fully exploit the great potential of open archives, giving us, in this particular case, a much more complete view of blazars. The work presented in this paper aims at being a step in this direction.

6 CONCLUSION

We have analysed the Swift-XRT data taken in PC and WT modes of 65 blazars observed at least 50 times from launch in late 2004 to the end of 2020. We have processed a total of 31 068 Swift-XRT observations and individual snapshots using a software pipeline called Swift_xrtproc that automatically retrieves the data, performs a spectral and photometric analysis, and writes the results to an archive database. This work complements and extends the results presented in Giommi et al. (2019) based on a X-ray imaging analysis of the blazars observed by Swift in PC mode. It represents another step towards the development of a multimessenger multitemporal high-transparency archive of blazars data products and results. We have used this unprecedented dataset to describe the general temporal and spectral behaviour of blazars of different types. Specific papers on timing analysis, spectral modeling, and neutrino emission prediction will be presented in the near future.

ACKNOWLEDGEMENTS

We acknowledge the use of data, analysis tools and services from the Open Universe platform, the ASI Space Science Data Center (SSDC), the Astrophysics Science Archive Research Center (HEASARC), the Astrophysics Data System (ADS), and the National Extra-galactic Database (NED).

PG acknowledges the support of the Technische Universität München – Institute for Advanced Studies, funded by the German Excellence Initiative (and the European Union Seventh Framework Programme under grant agreement number 291763) and the support by the Excellence Cluster ORIGINS, which is funded by the Deutsche Forschungsgemeinschaft (DFG, German Research Foundation) under Germany's Excellence Strategy – EXEC-2094 - 390783311.

CHB acknowledges the support of ICRANet and the Brazilian government, funded by the CAPES Foundation, Ministry of Education of Brazil under the project BEX 15113-13-2.

UBdA acknowledges the support of a CNPq Productivity Research grant number 311997/2019-8 and a Serrapilheira Institute grant number Serra – 1812-26906. He also acknowledges the receipt of a FAPERJ Young Scientist Fellowship number E-26/202.818/2019.

RM acknowledges the financial support of INAF (Istituto Nazionale di Astrofisica), Osservatorio Astronomico di Roma, ASI (Agenzia Spaziale Italiana) under contract to INAF: ASI 2014-049-R.0 dedicated to SSDC.

NS acknowledges the support by the Science Committee of RA, in the frames of the research project number 20TTCG-1C015.

We thank the referee for useful comments.

DATA AVAILABILITY

All results generated as part of this work are available through the tools and web pages of the Open Universe platform, e.g. the VOU-BLazars application (Chang et al. 2020) and the interactive table at https://openuniverse.asi.it/blazars/swift/, the ASI SSDC, the Virtual Observatory, and as a fits formatted file that can be downloaded at the following URL: https://openuniverse.asi.it/OU4Blazars/oublazars_swift_spectra_v1.0.fits.gz

REFERENCES

Abdo A. A. et al., 2010, ApJ, 716, 30
Abdollahi S. et al., 2020, ApJS, 247, 33
Arnaud K. A., 1996, in Jacoby G. H., Barnes J., eds, ASP Conf. Ser. Vol. 101, Astronomical Data Analysis Software and Systems V. Astron. Soc. Pac., San Francisco, p.17
Ballet J., Burnett T. H., Digel S. W., Lott B., 2020, preprint (arXiv:2005.11208)
Biteau J. et al., 2020, Nat. Astron., 4, 124
Blandford R., Rees M., 1978, in Wolfe A. M., ed., Pittsburgh Conf. BL Lac Objects. University of Pittsburgh Press, Pittsburgh, p. 341
Bonning E. et al., 2012, ApJ, 756, 13
Burrows D. N. et al., 2005, Space Sci. Rev., 120, 165
Cash W., 1979, ApJ, 228, 939
Chang Y. L., Arsioli B., Giommi P., Padovani P., Brandt C. H., 2019, A&A, 632, A77
Chang Y. L., Brandt C. H., Giommi P., 2020, Astron. Comput., 30, 100350
Consortium Cherenkov Telescope Array et al., 2019, Science with the Cherenkov Telescope Array. World Scientific Publishing Co. Pte. Ltd.
Ciprini S., Cheung C. C., Kocevski D., Chiang J., Fermi Large Area Telescope Collaboration, Shore S. N., 2017, The Astronomer's Telegram, 10482, 1
Falomo R., Pian E., Treves A., 2014, A&A Rev., 22, 73
Gehrels N. et al., 2004, ApJ, 611, 1005
George I. M., Warwick R. S., Bromage G. E., 1988, MNRAS, 232, 793
Giommi P., 2015, Journal of High Energy Astrophysics, 7, 173
Giommi P., Barr P., Garilli B., Maccagni D., Pollock A. M. T., 1990, ApJ, 356, 432
Giommi P., Padovani P., Perlman E., 2000, MNRAS, 317, 743
Giommi P. et al., 2008, A&A, 487, L49
Giommi P. et al., 2012, A&A, 541, A160
Giommi P. et al., 2019, A&A, 631, A116 (Paper I)
Giommi P. et al., 2020a, in Ferretti S., ed., Space Capacity Building in the XXI Century. Studies in Space Policy. Springer, p. 377
Giommi P., Glauch T., Padovani P., Resconi E., Turcati A., Chang Y. L., 2020b, MNRAS, 497, 865
Giommi P. et al., 2020c, A&A, 642, A141
Grandi P., Palumbo G. G. C., 2004, Science, 306, 998
Humphrey P. J., Liu W., Buote D. A., 2009, ApJ, 693, 822
IceCube Collaboration et al., 2018, Science, 361, 147
Kapanadze B., Dorner D., Vercellone S., Romano P., Kapanadze S., Mdzinarishvili T., 2016a, MNRAS, 461, L26
Kapanadze B. et al., 2016b, ApJ, 831, 102
Kapanadze B., Dorner D., Romano P., Vercellone S., Kapanadze S., Tabagari L., 2017, ApJ, 848, 103
Kapanadze B. et al., 2018a, ApJS, 238, 13
Kapanadze B. et al., 2018b, MNRAS, 473, 2542
Kapanadze B. et al., 2018c, ApJ, 854, 66
Kapanadze B., Vercellone S., Romano P., Hughes P., Aller M., Aller H., Kharshiladze O., Tabagari L., 2018d, ApJ, 858, 68
Kapanadze B. et al., 2020, ApJS, 247, 27
La Mura G., Chiaro G., Conceição R., De Angelis A., Pimenta M., Tomé B., 2020, MNRAS, 497, 3142
Mannheim K., 1995, Astropart. Phys., 3, 295
Massaro E., Tramacere A., Perri M., Giommi P., Tosti G., 2006, A&A, 448, 861
Massaro E., Maselli A., Leto C., Marchegiani P., Perri M., Giommi P., Piranomonte S., 2015, Ap&SS, 357, 75
Merloni A. et al., 2012, preprint (arXiv:1209.3114)
Merloni A., Nandra K., Predehl P., 2020, Nat. Astron., 4, 634
Morini M., Chiappetti L., Maccagni D., Maraschi L., Molteni D., Tanzi E. G., Treves A., Wolter A., 1986, ApJ, 306, L71
Morokuma T. et al., 2020, preprint (arXiv:2011.04957)
Padovani P., Giommi P., 1995, ApJ, 444, 567
Padovani P. et al., 2017, A&A Rev., 25, 2
Padovani P., Giommi P., Resconi E., Glauch T., Arsioli B., Sahakyan N., Huber M., 2018, MNRAS, 480, 192
Pian E. et al., 1998, ApJ, 492, L17
Resconi E., Coenders S., Padovani P., Giommi P., Caccianiga L., 2017, MNRAS, 468, 597
Sahakyan N., Giommi P., 2021, MNRAS, 502, 836
Urry C. M., Padovani P., 1995, PASP, 107, 803
Vaughan S. et al., 2006, ApJ, 638, 920
Voges W. et al., 1999, A&A, 349, 389
Wang Y., Xue Y., Zhu S., Fan J., 2018, ApJ, 867, 68
Xiong D. et al., 2020, ApJS, 247, 49

This paper has been typeset from a TEX/LATEX file prepared by the author.